Spin-Orbit Interaction and Induced Superconductivity in a One-Dimensional Hole Gas

De Vries, Folkert K.; Shen, Jie; Skolasinski, Rafal J.; Nowak, Michal P.; Varjas, Daniel; Wang, Lin; Wimmer, Michael; Zwanenburg, Floris A.; Li, Ang; Koelling, Sebastian

DOI
10.1021/acs.nanolett.8b02981

Publication date
2018

Document Version
Final published version

Published in
Nano Letters

NANO LETTERS

Letter

Cite This: Nano Lett. 2018, 18, 6483−6488

pubs.acs.org/NanoLett

Spin−Orbit Interaction and Induced Superconductivity in a One-Dimensional Hole Gas

Folkert K. de Vries,[#,†] Jie Shen,[#,*,†] Rafal J. Skolasinski,[†] Michal P. Nowak,[‡] Daniel Varjas,[†] Lin Wang,[†] Michael Wimmer,[†] Joost Ridderbos,[¶] Floris A. Zwanenburg,[¶] Ang Li,[§,○] Sebastian Koelling,[§] Marcel A. Verheijen,[§,∥] Erik P. A. M. Bakkers,[§] and Leo P. Kouwenhoven[*,†,⊥]

[†]QuTech and Kavli Institute of Nanoscience, Delft University of Technology, 2600 GA Delft, The Netherlands

[‡]AGH University of Science and Technology, Academic Centre for Materials and Nanotechnology, al. A. Mickiewicza 30, 30-059 Krakow, Poland

[¶]NanoElectronics Group, MESA and Institute for Nanotechnology, University of Twente, Enschede 7500 AE, The Netherlands

[§]Department of Applied Physics, Eindhoven University of Technology, Eindhoven 5600 MB, The Netherlands

[∥]Philips Innovation Laboratories, 5656 AE Eindhoven, The Netherlands

[⊥]Microsoft Station Q Delft, 2600 GA Delft, The Netherlands

Supporting Information

ABSTRACT: Low dimensional semiconducting structures with strong spin−orbit interaction (SOI) and induced superconductivity attracted great interest in the search for topological superconductors. Both the strong SOI and hard superconducting gap are directly related to the topological protection of the predicted Majorana bound states. Here we explore the one-dimensional hole gas in germanium silicon (Ge−Si) core−shell nanowires (NWs) as a new material candidate for creating a topological superconductor. Fitting multiple Andreev reflection measurements shows that the NW has two transport channels only, underlining its one-dimensionality. Furthermore, we find anisotropy of the Landé g-factor that, combined with band structure calculations, provides us qualitative evidence for the direct Rashba SOI and a strong orbital effect of the magnetic field. Finally, a hard superconducting gap is found in the tunneling regime and the open regime, where we use the Kondo peak as a new tool to gauge the quality of the superconducting gap.

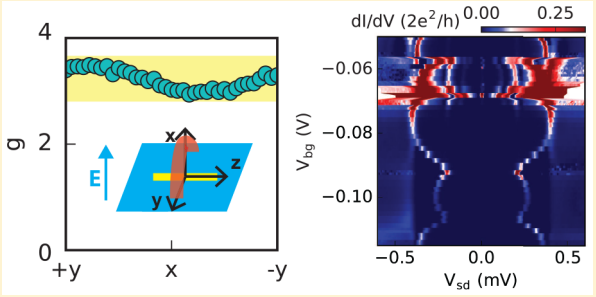

KEYWORDS: *Spin−orbit interaction, g-factor anisotropy, Josephson junction, multiple Andreev reflection, nanowires, hole transport*

The large band offset and small dimensions of the Ge−Si core−shell nanowire (NW) lead to the formation of a high-quality one-dimensional hole gas.[1,2] Moreover, the direct coupling of the two lowest-energy hole bands mediated by the electric field is predicted to lead to a strong direct Rashba spin−orbit interaction (SOI).[3,4] The bands are coupled through the electric dipole moments that stem from their wave function consisting of a mixture of angular momentum (L) states. On top of that, the spin states of that wave function are mixed due to heavy and light hole mixing. Therefore, an electric field couples via the dipole moment to the spin states of the system and causes the SOI. This is different from the Rashba SOI, which originates from the coupling of valence and conduction bands. The predicted strong SOI is interesting for controlling the spin in a quantum dot electrically.[5,6] Combining this strong SOI with superconductivity is a promising route toward a topological superconductor.[7,8] Signatures of Majorana bound states (MBSs) have been found in multiple NW experiments.[9,10] An important intermediate result is the measurement of a hard superconducting gap,[11,12] which ensures the semiconductor is well proximitized as is needed for obtaining MBSs.

Here we study a superconducting quantum dot in a Ge−Si NW. The scanning and transmission electron microscopy images of the device (Figure 1a,b) show a Josephson junction of ∼170 nm in length. The quantum dot is formed in between the contacts. The Ge−Si core−shell nanowires were grown by the vapor−liquid−solid (VLS) method as discussed in detail in the Supporting Information of ref 2. The NW has a Ge core with a radius of 3 nm. The Ge crystal direction is found to be [110], in which hole mobilities up to 4600 cm^2/Vs are reported.[2] The elemental analysis in Figure 1c reveals a pure Ge core with a 1 nm Si shell and a 3 nm amorphous silicon oxide shell around the wire. Superconductivity is induced in the Ge core by aluminum (Al) leads,[13] and crucially, the device is annealed for a short time at a moderate temperature.[14,15] We

Received: July 21, 2018
Revised: August 23, 2018
Published: September 7, 2018

DOI: 10.1021/acs.nanolett.8b02981
Nano Lett. 2018, 18, 6483−6488

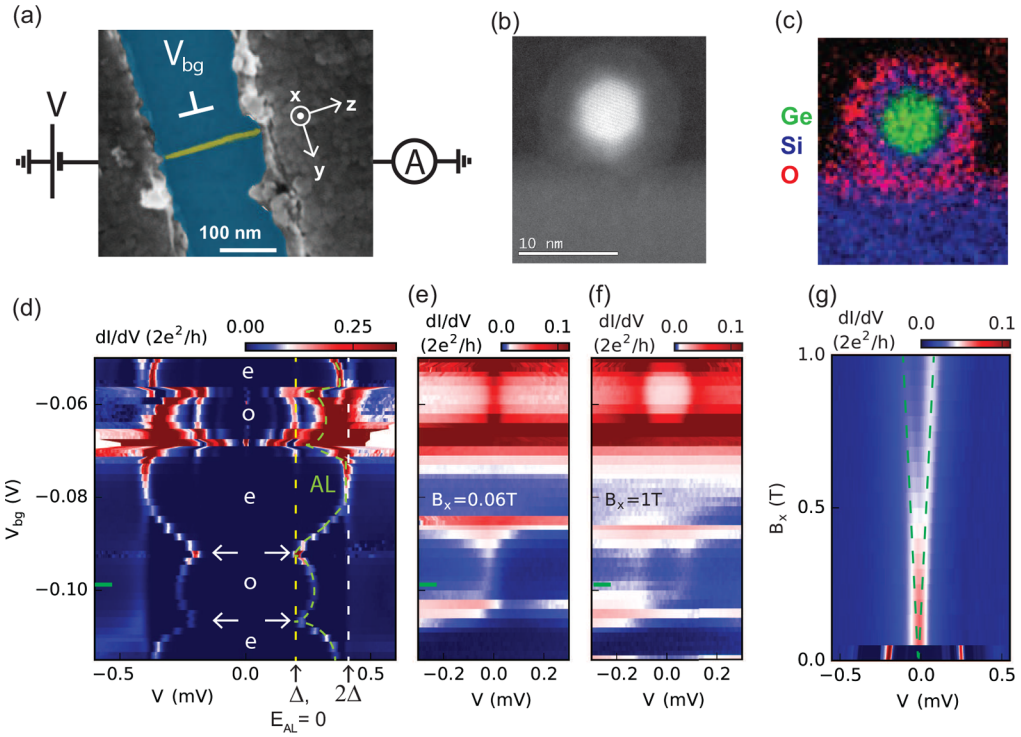

Figure 1. (a) False colored scanning electron microscope image of the device with the NW (yellow) with aluminum contacts (gray) on a Si/SiN_x wafer (blue). The magnetic field axes, voltage bias measurement setup, and global bottom gate are indicated. (b) Transmission electron microscope (TEM) image of the cross section of the NW. (c) Energy dispersive X-ray spectroscopy of the area displayed in panel b. The colors represent different elements: Ge is green, Si is blue, and oxygen (O) is red, respectively. The Ge−Si core−shell wire is capped by a SiO_x shell. (d) Voltage bias tunneling spectroscopy measurement of the superconducting quantum dot as the bottom gate voltage V_{bg} is altered. The superconducting gap, an Andreev level (AL), and multiple Andreev reflections appear as peaks in differential conductance (dI/dV). The AL, Δ, and 2Δ are marked by dashed green, yellow, and white lines, respectively. The even or odd occupation is indicated, and the kink in the observed Andreev level is highlighted by the arrows. (e, f) Same measurement as panel d with a magnetic field, B, applied perpendicular to the substrate (x-direction) of 60 mT and 1 T, respectively. A zero bias Kondo peak is observed as the quantum dot is occupied by an odd number of electrons. At B = 1 T, the resonance is split due to the Zeeman effect. (g) Linear splitting of the Kondo peak at V_{bg} = −0.098 V as a function of B. The Zeeman effect splits the spinful Kondo peak, which is indicated by the dashed green line.

believe that the high temperature causes the Al to diffuse in the wire, therefore enhancing the coupling to the hole gas. Note that we do not diffuse the Al all the way through, since we pinch off the wire (Figure S1) and there is no Al found in the elemental analysis (Figure 1c). Two terminal voltage bias measurements are performed on this device in a dilution refrigerator with an electron temperature of ∼50 mK.

To perform tunneling spectroscopy measurements, the bottom gate voltage V_{bg} is used to vary the barriers of the quantum dot and alter the density of the holes as well. From a large source-drain voltage, V, measurement (Figure S1), we estimate a charging energy, U, of 12 meV, barriers' asymmetry of Γ_1/Γ_2 = 0.2−0.5, where $\Gamma_{1(2)}$ is the coupling to the left (right) lead, and a lever arm of 0.3 eV/V. In Figure 1d, the differential conductance dI/dV as a function of V versus V_{bg} reveals a superconducting gap (2Δ = 380 μeV) and several Andreev processes within this window. Additionally, an even−odd structure shows up in both the superconducting state at low V and normal state at high V, which is related to the even or odd parity of the holes in the quantum dot. The even−odd structure persists as we suppress the superconductivity in the device by applying a small magnetic field (60 mT) perpendicular to the substrate (Figure 1e). A zero bias peak appears when the quantum dot has odd parity. This is a signature of the Kondo effect.[16,17] When increasing the magnetic field to 1 T, the Kondo peak splits due to the Zeeman effect by $2g\mu_B B$. The energy splitting of the two levels is linear as shown in Figure 1g and thus can be used to extract a Landé g-factor, g, of 1.9. In the remainder of the Letter, we will discuss the three magnetic field regimes of Figure 1d−f (0 T, 60 mT, and 1T, respectively) in more detail.

The resonance that disperses with V_{bg} in Figure 1d is an Andreev Level (AL), which is the energy transition from the ground to the excited state in the dot.[18,19] The ground state of the dot switches between singlet and doublet if the occupation in the dot changes, as sketched in the phase diagram in the top panel of Figure 2a. Since our charging energy is large, we trace the dashed line in the phase diagram. The AL undergoes Andreev reflection at the side of the quantum dot with a large coupling (Γ_2) and normal reflection at the opposite side that has lower coupling (Γ_1), as schematically drawn in the bottom panel of Figure 2a. The superconducting lead with the low coupling serves as a tunneling spectroscopy probe of the density of states. To be more precise, the coherence peak of the superconducting gap probes the Andreev level energy, E_{AL}. For example, if E_{AL} = 0, we measure it at eV = Δ; the resonance thus has an offset of ±Δ in the measurement in Figure 1d. The ground state transition is visible as a kink of the resonance at V = Δ at V_{bg} = −0.09 and −0.11 mV. At a more negative V_{bg}, the coupling of the hole gas to the superconducting reservoirs is strongly enhanced. This eventually

DOI: 10.1021/acs.nanolett.8b02981
Nano Lett. 2018, 18, 6483−6488

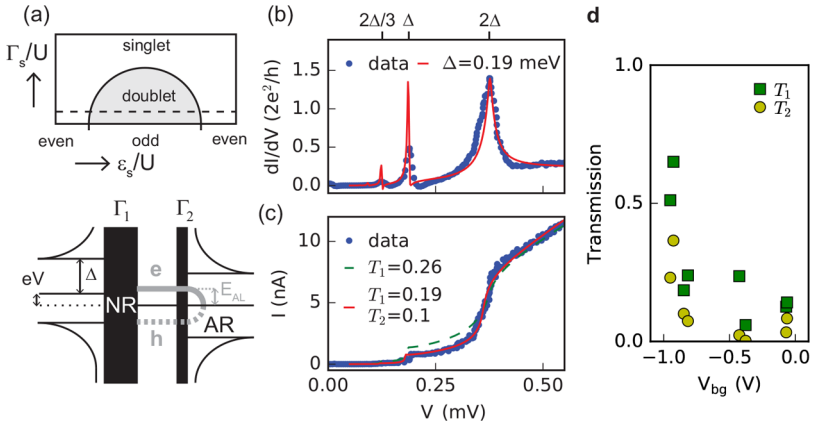

Figure 2. (a, top) A phase diagram of the ground state in the superconducting quantum dot sketched as a function of the quantum dot energy ϵ_0 versus the coupling to the superconducting reservoir Γ_s, both normalized to the charging energy, U. Because of the large U compared to Γ_s, we expect to trace the dashed line. The bottom panel shows the Andreev level (dashed gray line) with energy E_{AL} that is formed by the Andreev reflection (AR) at one side and normal reflection (NR) at the other side of the dot. The reflection processes are different due to asymmetric barriers Γ_1 and Γ_2, indicated as the barrier width. The density of states in the NW is probed by the superconductor on the left side by doing voltage bias tunneling spectroscopy. (b) Tunneling spectroscopy measurement at $V_{bg} = -0.85$ V. The first- and second-order multiple Andreev reflections are observed. A two-mode model fits the data well with $\Delta = 190$ μeV. (c) Measured current of panel b. The data is fitted with a single- and two-mode model. The latter resembles the data better and is therefore used to extract transmission values. (d) Transmission of the first and second mode, T_1 and T_2, extracted from the fit of multiple Andreev reflections at a different V_{bg}. The transmission increases significantly below $V_{bg} = -0.8$ V.

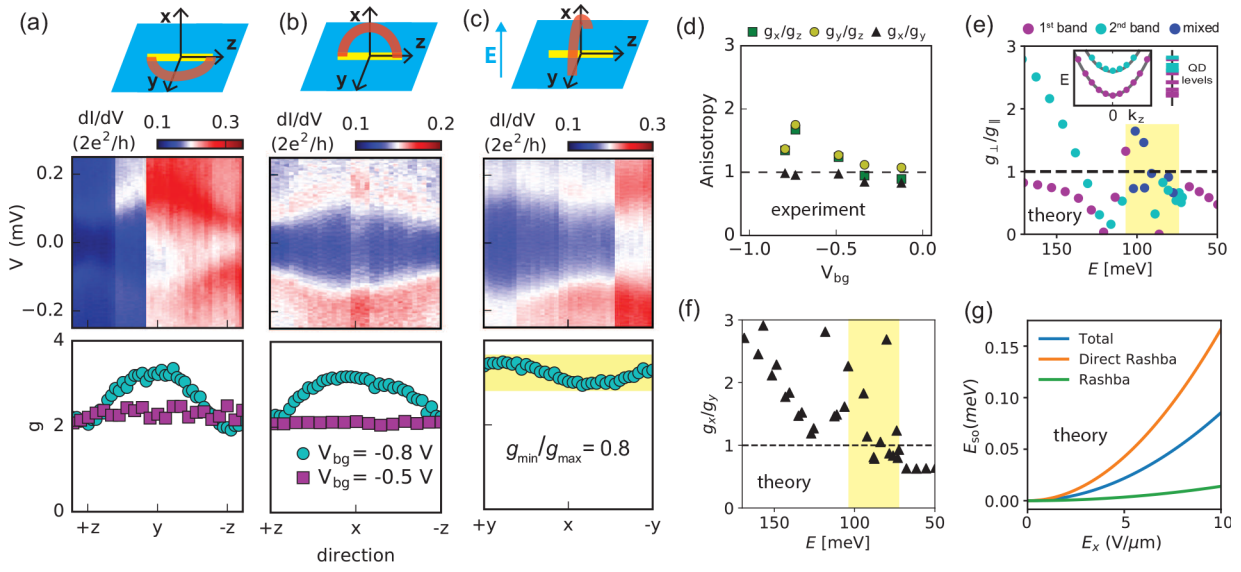

Figure 3. (a–c) Rotations of the magnetic field with a 0.9 T magnitude in the *yz*-, *xz*-, and *xy*-plane, respectively, at $V_{bg} = -0.79$ V. The upper panel shows the schematic of the device and the magnetic field rotation performed. The differential conductance data is plotted in the center panel, and the splitting of the Kondo peak changes as the angles are swept. The sudden changes in conductance are due to small switches in V_{bg}. The lower panel shows the extracted g of the center panel in cyan and g at $V_{bg} = -0.5$ V in magenta. For the *xy*-plane. the anisotropy is highlighted and calculated. (d) Summary of the measured anisotropies of g at a different V_{bg}. (e) Simulation result of the quantum dot. The anisotropy of $g_{\parallel}$ and $g_{\perp}$ changes as the Fermi energy is altered. The colors represent the band from where the quantum dot level predominantly stems. The highlighted part shows a similar behavior in the anisotropy values as the data in part d. The inset depicts a schematic representation of the energy ordering of the quantum dot levels originating from two bands along the NW. (f) Simulation as in part e, now with an applied electric field of 10 V/μm. The SOI causes anisotropy with respect to the electric field direction as g_x is pointed perpendicular and g_y parallel to the electric field. The anisotropy increases as the Fermi level is raised. The same range as in part e is highlighted. (g) Simulated spin–orbit energies for the first band ($k = 0$) of the infinite wire model as a function of the electric field along the x-direction. The direct Rashba term is the leading contribution.

leads to the observation of both the DC and AC Josephson effects (Figure S2).

In the upper part of Figure 1d, we measure the multiple Andreev reflection (MAR): resonances at integer fractions of the superconducting gap. Figure 2b presents a line trace at $V_{bg} = -0.85$ V that shows the gap edge and first- and second-order Andreev reflection. Fitting the differential conductance[20,21] (see Supporting Information) allows us to extract $\Delta = 190$ μeV, close to the bulk gap of Al. We also fit the measured current to extract the transmission of the spin degenerate longitudinal modes in the NW (Figure 2c).[22,23] The two-mode fit resembles the data better than the single-mode fit. Also, we checked that fitting with more than two-modes results in $T = 0$ outcomes for the extra modes. Therefore, the first provides us

DOI: 10.1021/acs.nanolett.8b02981
Nano Lett. 2018, 18, 6483–6488

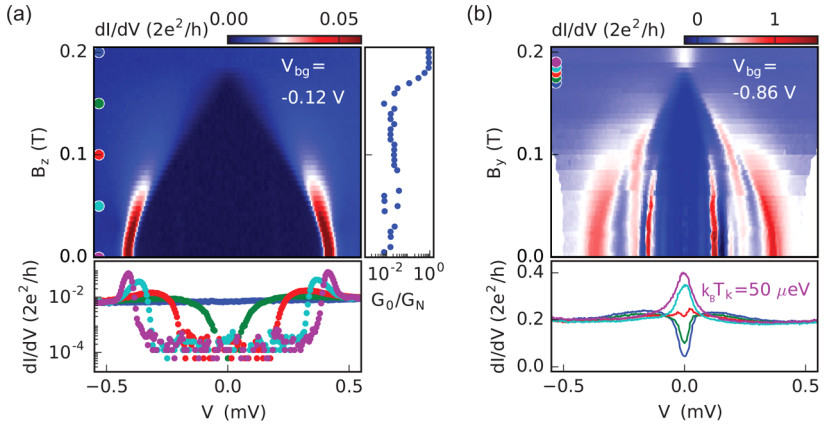

Figure 4. (a) Closing of the superconducting gap, as B is ramped up in the z-direction. The line traces below are taken at 50 mT intervals and show the induced superconducting gap. The vertical line trace shows the conductance at $V = 0$ V normalized to the conductance extracted at $V = 0.5$ mV. A 2 orders of magnitude conductance suppression is observed. (b) The superconducting gap closes, and a Kondo peak appears as the magnetic field is increased in the y-direction. The resonances within the gap stem from Andreev processes. The line traces depict the transition from the superconducting gap to the Kondo peak, which takes place from 170 to 190 mT (5 mT step). From the pink trace, a Kondo energy k_BT_K of 50 μeV is extracted with a Lorentzian fit.

with an estimate for the transmission in the two modes, T_1 and T_2. We interpret the two modes as two semiconducting bands in the NW. The MAR fitting analysis is repeated at a different V_{bg}, and the resulting T_1 and T_2 are plotted in Figure 2d. The strong increase of the transmission below $V_{bg} = -0.8$ V is attributed to the increase of the Fermi level and Γ_1 and Γ_2.

The Landé g-factor g is investigated further by measuring the Kondo peak splitting as a 0.9 T magnetic field is rotated from y- to z-, x- to z-, and x- to y-direction as presented in the second row of Figure 3a−c. Interestingly, we find a strong anisotropy of the Kondo peak splitting and accordingly of g at $V_{bg} = -0.79$ V and $V_{bg} = -0.82$ V; see the bottom row of Figure 3a−c and Figure S4, respectively. Both directions perpendicular to the NW show a strongly enhanced g. Similar anisotropy has been reported before in a closed quantum dot, where g is even quenched in the z-direction.[24−26] In our experiment, the highest g of 3.5 is found when the magnetic field is pointed perpendicular to the NW and almost perpendicular to the substrate.

On the contrary, at a $V_{bg} = -0.5$ V, we find an isotropic g (bottom row of Figure 3a−c), all of which have a value of around 2. The anisotropies at a different V_{bg} are summarized in Figure 3d. The strong anisotropy seems to set in around $V_{bg} = -0.7$ V. This sudden transition from isotropic to anisotropic g, which has not been observed before in a quantum dot system, is correlated with the increase in transmission in Figure 2d. We speculate that the change from isotropic to anisotropic behavior is related to the occupation of two bands in the NW. To test this hypothesis and get an understanding of the origin of the anisotropy, we theoretically model the band structure of our NW and focus on the two lowest bands.

We use the model described in ref 4 and apply it to our experimental geometry (see Supporting Information for details). Simulating the device as an infinite wire, we first consider the anistropy of g between the directions parallel and perpendicular to the NW. We find that there are two contributions to the anisotropy: the Zeeman and the orbital effect of the magnetic field.[27,28] The anisotropy of the Zeeman component is similar for the two lowest bands, where for the orbital part the anisotropy differs strongly. The anisotropy of the total g, therefore, shows a strong difference for the two lowest bands (Figures S6 and S7). This agrees qualitatively with earlier predictions,[3] but we find additionally that strain lifts the quenching of g along the NW such that $g_{\parallel}/g_{\perp} \sim 2$, in agreement with our measurements. From these observations, we conclude that the observed isotropic and anisotropic g with respect to the NW-axis is due to the orbital effect.

In addition, we include the confinement along the NW, such that a quantum dot is formed and the energy levels are quantized in the z-direction. Besides the lowest-energy states studied before,[6,24] we also consider a large range of higher quantum dot levels. In the regime where two bands are occupied, we observe that the quantum dot levels originating from the first and second band have a unique ordering as a function of Fermi energy, this situation is sketched in the inset of Figure 3e. We also find that some of the quantum dot levels are a mixture of the two bands (Figure S9), resulting in a different anisotropy for each quantum dot level. In the simulation results (Figure 3e and Figure S10), the anisotropy values are colored according to the band they predominantly originate from. To compare the simulation with the measured data, we note that a more negative V_{bg} in the experiment increases the Fermi level for holes E. In the simulation, we observe a regime in E (highlighted in Figure 3e), where the anisotropy $g_{\perp}/g_{\parallel}$ is around 1 and goes up toward 2 as E increases. This behavior qualitatively resembles the measurement of g_x/g_z and g_y/g_z in Figure 3d.

Now we turn to the magnetic field rotation in the xy-plane, the two directions perpendicular to the NW that are parallel and perpendicular to the electric field induced by the bottom gate. The measured anisotropy is $g_{min}/g_{max} = 0.8$ (Figure 3c). The maximum g of 3.5 is just offset of the y-direction, which is almost parallel to the electric field. This anisotropy with respect to the electric field direction is a signature of the SOI.[24,25] As discussed before, the Ge−Si NWs are predicted to have both the Rashba SOI and the direct Rashba SOI.[3,6] The electric field could also cause anisotropy via the orbital effect or geometry, due to an anisotropic wave function. However, we can rule that out since our simulations show that the wave function does not significantly change as electric field is applied (Figure S8). In the simulation (Figure 3f) with a constant electric field of 10 mV/μm, we observe anisotropy of g parallel

DOI: 10.1021/acs.nanolett.8b02981
Nano Lett. 2018, 18, 6483−6488

(g_x) and perpendicular (g_y) to the electric field. Similar to our data, the anisotropy starts below 1 and goes to 1 as the Fermi level is increased. The spread in the anisotropy values is due to the mixing of the bands for each quantum dot level. Furthermore, we calculated the magnitude of the Rashba and direct contribution to the SOI using the infinite wire model and found that the direct Rashba SOI is dominating in the small diameter nanowires of our study (Figure 3g). This agrees with the effective Hamiltonian derived in ref 3, which predicts that the direct Rashba SOI dominates in NWs with a Ge core of 3 nm radius. To summarize, we observe anisotropy with respect to the electric field direction that is caused by the SOI, which is likely for the largest part due to the direct Rashba SOI.

Finally, in Figure 4, we take a detailed look at the superconducting gap as a function of magnetic field. We find the critical magnetic field B_c for different directions: $B_{c,z}$ = 220 mT (Figure 4a), $B_{c,y}$ = 220 mT (Figure 4b), and $B_{c,x}$ = 45 mT (Figure 1g and Figure S3), consistent with an Al thin film. Future devices could be improved by using a thinner Al film to increase the critical magnetic field.[29] In this case, the topological phase could be reachable, with the measured g of 3.5[8]. In the tunneling regime at V_{bg} = −0.12 V, we observe a clean gap closing (Figure 4a). The conductance inside the gap is suppressed by 2 orders of magnitude, signaling a low quasiparticle density of states in the superconducting gap. This large conductance suppression remains as the gap size decreases toward B_c (bottom panel in Figure 4a). In the low conductance regime, we thus measure a hard superconducting gap persisting up to B_c in Ge−Si NWs.

The closing of the superconducting gap in a higher conductance regime is presented in Figure 4b. Since the transmission is increased, Andreev reflection processes cause a significant conductance within the superconducting gap.[30] Therefore, the conductance suppression in the gap becomes an ill-defined measure of the quasiparticle density of states and with that the quality of the induced superconductivity. However, here we can use the Kondo peak to examine the quasiparticle density of states in the superconducting gap. The Kondo peak is formed by coupling through quasiparticle states within the window of the Kondo energy (k_BT_K). In the regime where $k_BT_K \leq \Delta$, the existence and size of the Kondo peak are then an indication of the quasiparticle density of states inside the superconducting gap.[31,32] In our measurement, Δ is indeed largerthan k_BT_K up to a magnetic field B = 170 mT (see the blue and magenta line traces in the bottom panel of Figure 4b). Since in the measurement the Kondo peak only arises once the gap is fully closed, we have a low quasiparticle density of states within the superconducting gap. This supports our observation of a hard superconducting gap up to B_c. It also illustrates a new way of gauging whether the superconducting gap is hard in a high conductance regime.

Combining all three magnetic field regimes of Figures 2−4, we observed Andreev levels showing a ground state transition, SOI from the coexistence of two bands in Ge−Si core−shell NWs, and a hard superconducting gap. The combination and correlation of these observations is a crucial step for exploring this material system as a candidate for creating a one-dimensional topological superconductor.

■ ASSOCIATED CONTENT

Supporting Information

The Supporting Information is available free of charge on the ACS Publications website at DOI: 10.1021/acs.nanolett.8b02981.

Experimental data and a description and intermediate results of the band structure calculations (PDF)

■ AUTHOR INFORMATION

Corresponding Authors

*E-mail: j.shen-1@tudelft.nl.

*E-mail: l.p.kouwenhoven@tudelft.nl. Phone: +31-15-27-81798.

ORCID

Jie Shen: 0000-0002-7205-5081

Sebastian Koelling: 0000-0002-6606-9110

Erik P. A. M. Bakkers: 0000-0002-8264-6862

Present Address

○Ang Li: Beijing Key Lab of Microstructure and Property of Advanced Materials, Beijing University of Technology, Pingleyuan No. 100, Beijing 100024, People's Republic of China

Author Contributions

#F.K.d.V. and J.S. contributed equally, designed the experiment, fabricated the devices, and performed the measurements. M.P.N. and M.W. did the MAR fitting. R.S., D.V., L.W., and M.W. performed band structure calculations. J.R. and F.Z. contributed to the discussions of data. A.L. and E.P.A.M.B. grew the material. S.K. and M.A.V. did TEM analysis. L.P.K. and J.S. supervised the project. F.K.d.V., J.S., R.S. and D.V. wrote the manuscript. All authors commented on the manuscript.

Notes

The authors declare no competing financial interest.

■ ACKNOWLEDGMENTS

The authors thank M. C. Cassidy for fruitful discussions about the fabrication and Y. Ren for help with the growth. This work has been supported by funding from the Netherlands Organization for Scientific Research (NWO), Microsoft Corporation Station Q, and European Research Council (ERC HELENA 617256 and ERC Starting Grant 638760). We acknowledge Solliance, a solar energy R&D initiative of ECN, TNO, Holst, TU/e, imec, and Forschungszentrum Jülich, and the Dutch province of Noord-Brabant for funding the TEM facility. M.P.N. acknowledges support by the National Science Centre, Poland (NCN) according to decision DEC-2016/23/D/ST3/00394.

■ REFERENCES

(1) Xiang, J.; Lu, W.; Hu, Y.; Wu, Y.; Yan, H.; Lieber, C. M. Ge/Si nanowire heterostructures as high-performance field-effect transistors. *Nature* **2006**, *441*, 489.

(2) Conesa-Boj, S.; Li, A.; Koelling, S.; Brauns, M.; Ridderbos, J.; Nguyen, T. T.; Verheijen, M. A.; Koenraad, P. M.; Zwanenburg, F. A.; Bakkers, E. P. A. M. Boosting Hole Mobility in Coherently Strained [110]-Oriented Ge-Si Core-Shell Nanowires. *Nano Lett.* **2017**, *17*, 2259−2264.

(3) Kloeffel, C.; Trif, M.; Loss, D. Strong spin-orbit interaction and helical hole states in Ge/Si nanowires. *Phys. Rev. B: Condens. Matter Mater. Phys.* **2011**, *84*, 195314.

DOI: 10.1021/acs.nanolett.8b02981
Nano Lett. 2018, 18, 6483−6488

(4) Kloeffel, C.; Rančić, M. J.; Loss, D. Direct Rashba spin-orbit interaction in Si and Ge nanowires with different growth directions. *Phys. Rev. B: Condens. Matter Mater. Phys.* **2018**, *97*, 235422.
(5) Nadj-Perge, S.; Frolov, S. M.; Bakkers, E. P. A. M.; Kouwenhoven, L. P. Spin-orbit qubit in a semiconductor nanowire. *Nature* **2010**, *468*, 1084−7.
(6) Kloeffel, C.; Trif, M.; Stano, P.; Loss, D. Circuit QED with hole-spin qubits in Ge/Si nanowire quantum dots. *Phys. Rev. B: Condens. Matter Mater. Phys.* **2013**, *88*, 241405.
(7) Alicea, J. New directions in the pursuit of Majorana fermions in solid state systems. *Rep. Prog. Phys.* **2012**, *75*, 076501.
(8) Maier, F.; Klinovaja, J.; Loss, D. Majorana fermions in Ge/Si hole nanowires. *Phys. Rev. B: Condens. Matter Mater. Phys.* **2014**, *90*, 195421.
(9) Mourik, V.; Zuo, K.; Frolov, S. M.; Plissard, S. R.; Bakkers, E. P. A. M.; Kouwenhoven, L. P. Signatures of Majorana Fermions in Hybrid Superconductor-Semiconductor Nanowire Devices. *Science* **2012**, *336*, 1003−1007.
(10) Deng, M. T.; Vaitiekenas, S.; Hansen, E. B.; Danon, J.; Leijnse, M.; Flensberg, K.; Nygård, J.; Krogstrup, P.; Marcus, C. M. Majorana bound state in a coupled quantum-dot hybrid-nanowire system. *Science* **2016**, *354*, 1557−1562.
(11) Chang, W.; Albrecht, S.; Jespersen, T.; Kuemmeth, F.; Krogstrup, P.; Nygård, J.; Marcus, C. M. Hard gap in epitaxial semiconductor-superconductor nanowires. *Nat. Nanotechnol.* **2015**, *10*, 232−6.
(12) Gül, Ö.; et al. Hard Superconducting Gap in InSb Nanowires. *Nano Lett.* **2017**, *17*, 2690−2696.
(13) Xiang, J.; Vidan, A.; Tinkham, M.; Westervelt, R. M.; Lieber, C. M. Ge/Si nanowire mesoscopic Josephson junctions. *Nat. Nanotechnol.* **2006**, *1*, 208−13.
(14) Su, Z.; Zarassi, A.; Nguyen, B.-M.; Yoo, J.; Dayeh, S.; Frolov, S. High critical magnetic field superconducting contacts to Ge/Si core/shell nanowires. 2016, arXiv:1610.03010. *arXiv.org e-Print archive*. https://arxiv.org/abs/1610.03010.
(15) Ridderbos, J.; Brauns, M.; Shen, J.; de Vries, F. K.; Li, A.; Bakkers, E. P. A. M.; Brinkman, A.; Zwanenburg, F. A. Josephson effect in a few-hole quantum dot. *Adv. Mater.* **2018**, 1802257.
(16) Goldhaber-Gordon, D.; Shtrikman, H.; Mahalu, D.; Abusch-Magder, D.; Meirav, U.; Kastner, M. Kondo effect in a single-electron transistor. *Nature* **1998**, *391*, 156.
(17) Cronenwett, S. M.; Oosterkamp, T. H.; Kouwenhoven, L. P. A Tunable Kondo Effect in Quantum Dots. *Science* **1998**, *281*, 540−544.
(18) Deacon, R. S.; Tanaka, Y.; Oiwa, A.; Sakano, R.; Yoshida, K.; Shibata, K.; Hirakawa, K.; Tarucha, S. Tunneling Spectroscopy of Andreev Energy Levels in a Quantum Dot Coupled to a Superconductor. *Phys. Rev. Lett.* **2010**, *104*, 076805.
(19) Lee, E.; Jiang, X.; Houzet, M.; Aguado, R.; Lieber, C.; De Franceschi, S. Spin-resolved Andreev levels and parity crossings in hybrid superconductor-semiconductor nanostructures. *Nat. Nanotechnol.* **2014**, *9*, 79−84.
(20) Averin, D.; Bardas, A. ac Josephson Effect in a Single Quantum Channel. *Phys. Rev. Lett.* **1995**, *75*, 1831−1834.
(21) Kjaergaard, M.; Suominen, H. J.; Nowak, M. P.; Akhmerov, A. R.; Shabani, J.; Palmstrøm, C. J.; Nichele, F.; Marcus, C. M. Transparent Semiconductor-Superconductor Interface and Induced Gap in an Epitaxial Heterostructure Josephson Junction. *Phys. Rev. Appl.* **2017**, *7*, 034029.
(22) Scheer, E.; Joyez, P.; Esteve, D.; Urbina, C.; Devoret, M. H. Conduction Channel Transmissions of Atomic-Size Aluminum Contacts. *Phys. Rev. Lett.* **1997**, *78*, 3535−3538.
(23) Goffman, M. F.; Urbina, C.; Pothier, H.; Nygård, J.; Marcus, C.; Krogstrup, P. Conduction channels of an InAs-Al nanowire Josephson weak link. *New J. Phys.* **2017**, *19*, 092002.
(24) Maier, F.; Kloeffel, C.; Loss, D. Tunable gfactor and phonon-mediated hole spin relaxation in Ge/Si nanowire quantum dots. *Phys. Rev. B: Condens. Matter Mater. Phys.* **2013**, *87*, No. 161305(R).
(25) Brauns, M.; Ridderbos, J.; Li, A.; Bakkers, E. P. A. M.; Zwanenburg, F. A. Electric-field dependent g-factor anisotropy in Ge-Si core-shell nanowire quantum dots. *Phys. Rev. B: Condens. Matter Mater. Phys.* **2016**, *93*, No. 121408(R).
(26) Brauns, M.; Ridderbos, J.; Li, A.; Bakkers, E. P. A. M.; van der Wiel, W. G.; Zwanenburg, F. A. Anisotropic Pauli spin blockade in hole quantum dots. *Phys. Rev. B: Condens. Matter Mater. Phys.* **2016**, *94*, 041411.
(27) Nijholt, B.; Akhmerov, A. R. Orbital effect of magnetic field on the Majorana phase diagram. *Phys. Rev. B: Condens. Matter Mater. Phys.* **2016**, *93*, 235434.
(28) Winkler, G. W.; Varjas, D.; Skolasinski, R.; Soluyanov, A. A.; Troyer, M.; Wimmer, M. Orbital Contributions to the Electron *g* Factor in Semiconductor Nanowires. *Phys. Rev. Lett.* **2017**, *119*, 037701.
(29) Shabani, J.; Kjaergaard, M.; Suominen, H. J.; Kim, Y.; Nichele, F.; Pakrouski, K.; Stankevic, T.; Lutchyn, R. M.; Krogstrup, P.; Feidenhans'l, R.; Kraemer, S.; Nayak, C.; Troyer, M.; Marcus, C. M.; Palmstrøm, C. J. Two-dimensional epitaxial superconductor-semiconductor heterostructures: A platform for topological superconducting networks. *Phys. Rev. B: Condens. Matter Mater. Phys.* **2016**, *93*, 155402.
(30) Blonder, G. E.; Tinkham, M.; Klapwijk, T. M. Transition from metallic to tunneling regimes in superconducting microconstrictions: Excess current, charge imbalance, and supercurrent conversion. *Phys. Rev. B: Condens. Matter Mater. Phys.* **1982**, *25*, 4515−4532.
(31) Buitelaar, M. R.; Nussbaumer, T.; Schonenberger, C. Quantum dot in the Kondo regime coupled to superconductors. *Phys. Rev. Lett.* **2002**, *89*, 256801.
(32) Lee, E.; Jiang, X.; Aguado, R.; Katsaros, G.; Lieber, C.; De Franceschi, S. Zero-Bias Anomaly in a Nanowire Quantum Dot Coupled to Superconductors. *Phys. Rev. Lett.* **2012**, *109*, 186802.

DOI: 10.1021/acs.nanolett.8b02981
Nano Lett. 2018, 18, 6483−6488